


Reflection and transmission of an incident solitary wave at an interface of a binary complex plasma in a microgravity condition

Xue-Ren Hong ¹, Wei Sun,² Mierk Schwabe ³, Cheng-Ran Du ^{2,*} and Wen-Shan Duan^{1,†}

¹College of Physics and Electronic Engineering, Northwest Normal University, 730070 Lanzhou, People's Republic of China

²College of Science, Donghua University, 201620 Shanghai, People's Republic of China

³Institut für Materialphysik im Weltraum, Deutsches Zentrum für Luft- und Raumfahrt (DLR), 82234 Weßling, Germany

 (Received 29 January 2021; revised 10 May 2021; accepted 6 August 2021; published 23 August 2021)

Theoretical results are given in the present paper, which can well explain the experimental observations performed under microgravity conditions in the PK-3 Plus Laboratory on board the International Space Station about the propagation of a solitary wave across an interface in a binary complex plasma. By using the traditional reductive perturbation method and the continuity conditions of both the electric potential and the momentum at the interface, we obtain the equivalent “initial conditions” for both the transmitted wave and the reflected waves from the incident wave. Then we obtain the numbers of the reflected and the transmitted solitary waves as well as all the wave amplitudes by using the inverse scattering method. The ripples of both reflection and transmission have also been given by using the Fourier series. The number of the reflected and the transmitted solitary waves produced by interface, as well as all the solitary wave amplitudes, depend on the system parameters such as the number density, electric charge, mass of the dust particles, and the effective temperature in both regions. The analytical results agree with observations in the experiments.

DOI: [10.1103/PhysRevE.104.025206](https://doi.org/10.1103/PhysRevE.104.025206)

I. INTRODUCTION

A complex plasma is a weakly ionized gas containing micro-sized solid particles which are highly charged by collecting ions and electrons and interact with each other via screened Coulomb interaction. It attracts extensively research interest because of its importance in understanding many space and astrophysics phenomena as well as the laboratory plasmas [1–4]. Complex plasmas show many low-frequency phenomena [5–7] due to the large mass of dust grains and almost have no impact on high-frequency oscillations [8–10].

Dust acoustic waves (DAW) were first reported theoretically in unmagnetized dusty plasmas by Rao *et al.* [3]. Shukla and Silin showed the existence of dust ion acoustic waves (DIAW) [9]. Laboratory experiments have confirmed the existence of DAW and DIAW [4,11,12]. Furthermore, low-frequency electrostatic ion acoustic and ion-cyclotron waves [13], dust lattice waves [14–17], rogue waves [18,19], magnetosonic waves [20], and shock waves [21,22] in complex plasmas have also been studied.

A binary complex plasma contains two types of microparticles of different sizes [23,24]. These two types of particles can either be mixed [25–28] or form a phase-separated system [29–32], caused by spinodal decomposition [31] or an imbalance of external forces [32]. In the latter case, an interface emerges between the separated phases. Recently, the propagation of self-excited waves and solitary waves has been discovered in the experiments performed in the PK-3 Plus

laboratory on board the International Space Station (ISS) [23,33]. The discovery of solitary waves goes back to Scott Russell in 1834. It was only with the derivation by Korteweg and de Vries in 1895 of what is now called the Korteweg de Vries (KdV) equation that the one soliton solution and hence the concept of solitary waves was put on a firm basis [34].

In addition, Langevin dynamics simulations have been performed to study the reflection and transmission of the solitary waves at the low damping regime, which was not realizable in the experiments due to the two-stream instability at low neutral gas pressure [35–38].

In this article, we conduct a theoretical investigation on the propagation of a solitary wave in a phase-separated binary complex plasma. By assuming that the complex plasma is a viscous fluid composed by microparticles, we give approximated analytical results of both the transmitted and the reflected waves due to the incident wave, using the reductive perturbation method. The analytical results are compared with the simulations and experiments and a qualitative agreements is found.

II. THEORETICAL MODEL

In order to understand the transmission and the reflection due to the incident wave at an interface, we consider a three components complex plasmas consisting of extremely massive, highly negatively charged inertial dust particles, inertialess Boltzmann distributed free electrons as well as inertialess Boltzmann distributed ions. Charge neutrality at equilibrium requires that $n_{i0} = Z_{d0}n_{d0} + n_{e0}$, where $n_{\alpha 0}$ is the unperturbed number density of the species α , $\alpha = e, i, d$ correspond to the electrons, ions, and dust particles, respectively,

*chengran.du@dhu.edu.cn

†duanws@nwnu.edu.cn

Z_{d0} is the number of charges of the electrons residing on the dust particle.

We use the equation of state of strongly coupled complex plasma proposed by Feng and his coworkers in a simple analytic expression [21,39–42]. The complex plasma pressure is the sum of a potential term and a kinetic term: $P = \alpha_d + \beta_d T_d$, where $\alpha_d = \frac{Q_d^2}{4\pi\epsilon_0\lambda_D^3} \{2.29 \exp[-2.45(a/\lambda_D)^2] + \frac{0.34}{(a/\lambda_D)^3}\}$ and $\beta_d = \frac{k_B}{\lambda_D^2} \{0.14 \exp[-0.37(a/\lambda_D)] + \frac{1.30}{(a/\lambda_D)^2}\}$ [39]. The first term α_d is attributed to the potential contribution of the particles, while the second term $\beta_d T$ comes from the kinetic contribution. We assume that the equation of state proposed by Feng is applicable for our model. Then we have the following equations in the international unit:

$$\frac{\partial n_d}{\partial t} + \frac{\partial(n_d u_d)}{\partial x} = 0, \quad (1)$$

$$\frac{\partial u_d}{\partial t} + u_d \frac{\partial u_d}{\partial x} = -\frac{Q_d}{m_d} \frac{\partial \phi}{\partial x} - \frac{1}{nm_d} \frac{\partial P}{\partial x} - \nu_d u_d, \quad (2)$$

$$\frac{\partial^2 \phi}{\partial x^2} = \frac{e}{\epsilon_0} (Z_{d0} n_d + n_e - n_i), \quad (3)$$

where n_d , u_d , m_d , P , and ν_d refer to the number density, the velocity, the mass, the pressure and the damping rate of the dust particles, respectively; $Q_d = -eZ_d$, where $Z_d > 0$ is the charge number of dust particles measured in unit of electron charge $-e$ and is assumed that it is a constant; $n_e = n_{e0} \exp(\frac{e\phi}{k_B T_e})$ and $n_i = n_{i0} \exp(-\frac{e\phi}{k_B T_i})$ are the electron number density with temperature T_e and the ion number density with temperature T_i ; ϕ is the electrostatic potential; and k_B is the Boltzmann constant.

For three-dimensional case, $a = n_d^{-1/3}$. The equation of state is actually $P = P(n_d, T_d)$, i.e., P is a function of both n_d and T_d . Then, we obtain a dispersion relation by assuming that the quantities of n_d , u_d , and ϕ vary in the form $\exp[i(kx - \omega t)]$,

$$\frac{\omega^2}{k^2} = n_{d0} \delta + \frac{n_{d0} Q_d^2}{\epsilon_0 m_d (\frac{1}{\lambda_{ie}^2} - k^2)}, \quad (4)$$

where $\delta = -\frac{1}{2} \frac{\kappa}{m_d v_{d0}^2} \frac{\partial P_d}{\partial \kappa}$, $\kappa = \frac{a}{\lambda_D}$, $\frac{\partial P_d}{\partial \kappa} = -\frac{Q_d^2}{4\pi\epsilon_0\lambda_D^3} [11.221 \exp(-2.45\kappa^2) + \frac{1.7}{\kappa^6}] - \frac{k_B T_d}{\lambda_D^2} [0.0518 \exp(-0.37\kappa) + \frac{2.6}{\kappa^3}]$, and $\lambda_{ie} = [\frac{n_{e0} e^2}{\epsilon_0 k_B T_e} + \frac{n_{i0} e^2}{\epsilon_0 k_B T_i}]^{1/2}$. For a long-wavelength approximation, $k\lambda_{ie} \ll 1$, we have the dust acoustic wave speed

$$C_d^2 = n_{d0} \delta + \frac{n_{d0} Q_d^2 \lambda_{ie}^2}{\epsilon_0 m_d}, \quad (5)$$

or

$$C_d^2 = n_{d0} \delta + \frac{k_B Z_{d0} T_{\text{eff}}}{m_d}, \quad (6)$$

where $T_{\text{eff}} = \frac{T_e T_i}{\mu T_e + \nu T_i}$ (effective temperature), $\nu = \frac{n_{e0}}{Z_{d0} n_{d0}}$, $\mu = \frac{n_{i0}}{Z_{d0} n_{d0}}$.

We now normalize all the physical quantities. The densities of electrons and ions are normalized by $Z_{d0} n_{d0}$, and the dust particle density is normalized by n_{d0} . Space coordinates x is normalized by the Debye length $\lambda_{Dd} = (\lambda_{Dd1}^2 + \lambda_{Dd2}^2)^{1/2}$, where $\lambda_{Dd1} = [\frac{n_{d0} \delta}{\omega_{pd}^2}]^{1/2}$, $\lambda_{Dd2} = (\frac{k_B Z_{d0} T_{\text{eff}}}{m_d \omega_{pd}^2})^{1/2}$, and $\beta = \frac{T_i}{T_e}$ is the

ratio of the ion temperature to electron temperature. Time t is normalized by the inverse of dusty plasma frequency $\omega_{pd}^{-1} = (\frac{2\epsilon_0 m_d}{n_{d0} Z_{d0}^2 e^2})^{1/2}$. Velocity is normalized by the dust acoustic speed C_d . The electrostatic potential ϕ is normalized by $\phi_0 = \frac{m_d C_d^2}{Q_d}$. Then the normalized equations are given by

$$\frac{\partial n}{\partial t} + \frac{\partial(nu)}{\partial x} = 0, \quad (7)$$

$$\frac{\partial u}{\partial t} + u \frac{\partial u}{\partial x} = \frac{\partial \phi}{\partial x} - \frac{\delta_p}{n^2} \frac{\partial P}{\partial x} - \nu_d u, \quad (8)$$

$$\frac{\partial^2 \phi}{\partial x^2} = \delta_\phi [n + \nu \exp(\beta s \phi) - \mu \exp(-s \phi)], \quad (9)$$

where $\delta_p = -\frac{\kappa}{2m_d n_{d0} C_d^2} \frac{\partial P}{\partial \kappa}$, $s = \frac{e\phi_0}{k_B T_i}$, and $\delta_\phi = \frac{n_{d0} Q_d \lambda_{Dd}^2}{\epsilon_0 \phi_0} = 2$.

Now we consider a model in which there are two regions. The plasma with smaller dust particles is in the region $x < 0$, while that with larger dust particles is in the region $x > 0$, i.e., the dusty plasma in the region $x < 0$ is different from that in the region $x > 0$. Suppose that there is an incident solitary wave propagating in the positive x direction in the region $x < 0$ initially. As it propagates, it will be reflected and transmitted at the interface $x = 0$. Due to this reason, we must consider both the reflected wave and the incident wave in the region $x < 0$, while we only need to consider the transmitted wave in the region $x > 0$. For simplicity, we use superscripts “ I ”, “ R ”, and “ T ” to represent the incident wave, the reflected wave, and the transmitted wave, respectively.

In order to understand the nonlinear solitary waves in the system, we will use the results of the inverse scattering method [43,44]. As is well known, the number of the solitary waves and their amplitudes can be given from the standard KdV equation and its “initial conditions” by using the inverse scattering method [43,44]. The “inverse scattering method” is a theoretical method to determine how many solitary waves are produced and what are their amplitude from an arbitrary initial condition.

For a standard KdV equation,

$$\frac{\partial \varphi}{\partial t} - 6\varphi \frac{\partial \varphi}{\partial \xi} + \frac{\partial^3 \varphi}{\partial \xi^3} = 0, \quad (10)$$

and its “initial condition,”

$$\varphi|_{t=0} = -\frac{A_0}{L_0^2} \text{sech}^2 \frac{\xi}{L_0}, \quad (11)$$

where $A_0 > 0$ is the characteristic width of the initial pulse, while A_0/L_0^2 is the characteristic amplitude of the initial pulse. The number N of generated solitary waves and their wave amplitudes for each solitary wave can be given by the inverse scattering method [43,44]. The number N is the maximum integer which satisfies [43,44],

$$\sqrt{A_0 + \frac{1}{4} + \frac{1}{2} - N} > 0 \quad (12)$$

and the amplitude of the j th generated solitary waves are

$$2 \left(\sqrt{A_0 + \frac{1}{4} + \frac{1}{2} - j} \right)^2 L_0^{-2}, \quad (13)$$

where $j = 1, 2, \dots, N$. However, it takes times to evolve solitary waves from an arbitrary initial condition.

We use the following reductive perturbation method [45–49] for the normalized equations of (7), (8), and (9):

$$\xi = \epsilon(x - v_s t) + \epsilon^2 P(\eta, \tau) + \dots, \quad (14)$$

$$\eta = \epsilon(x + v_s t) + \epsilon^2 Q(\xi, \tau) + \dots, \quad (15)$$

$$\tau = \epsilon^3 x, \quad (16)$$

where ϵ is a small parameter introduced in the perturbation process and ξ and η denote the trajectories of two solitary waves traveling in two different directions. Expand the physical quantities are as follows: $n = 1 + \epsilon^2 n_1 + \epsilon^4 n_2 + \dots$, $u = \epsilon^2 u_1 + \epsilon^4 u_2 + \dots$, and $\phi = \epsilon^2 \phi_1 + \epsilon^4 \phi_2 + \dots$. Substituting these equations into Eqs. (7), (8), and (9), we obtain the following equations in the lowest order (translated in the experimental coordinate):

$$\frac{n^I}{n_{d0}^-} = \frac{u^I}{C_D^-} = -\frac{\phi^I}{(T_{\text{eff}}^-/e)}, \quad (17)$$

$$\frac{n^R}{n_{d0}^-} = -\frac{u^R}{C_D^-} = -\frac{\phi^R}{(T_{\text{eff}}^-/e)}, \quad (18)$$

$$\frac{n^T}{n_{d0}^+} = \frac{u^T}{C_D^+} = -\frac{\phi^T}{(T_{\text{eff}}^+/e)}, \quad (19)$$

and in the next highest order, three KdV equations for the incident wave, the reflected wave, and the transmitted wave respectively as follows:

$$\frac{\partial \phi_1^I}{\partial \tau} + A^- \phi_1^I \frac{\partial \phi_1^I}{\partial \xi} + B^- \frac{\partial^3 \phi_1^I}{\partial \xi^3} = 0, \quad (20)$$

$$\frac{\partial \phi_1^R}{\partial \tau} + A^- \phi_1^R \frac{\partial \phi_1^R}{\partial \eta} + B^- \frac{\partial^3 \phi_1^R}{\partial \eta^3} = 0, \quad (21)$$

$$\frac{\partial \phi_1^T}{\partial \tau} + A^+ \phi_1^T \frac{\partial \phi_1^T}{\partial \xi} + B^+ \frac{\partial^3 \phi_1^T}{\partial \xi^3} = 0, \quad (22)$$

where $A^\pm = -\frac{3}{2} - \frac{\delta_p^\pm}{2(1-\delta_p^\pm)} - \frac{v^\pm(\beta^\pm)^2 - \mu^\pm}{2(\mu^\pm + v^\pm \beta^\pm)^2}$, $B^\pm = \frac{1}{4[s^\pm(\mu^\pm + v^\pm \beta^\pm)]^2}$, $\phi^\gamma = \epsilon^2 \phi_1^\gamma$, $\gamma = I, R, T$, ϕ^γ represent the electrostatic potential of the wave γ in the experimental coordinate, the superscript “-” represents the values in the region $x < 0$, while the superscript “+” represents the values in the region $x > 0$.

There are many solutions of Eqs. (20), (21), and (22). However, we are only interested in one solitary wave solution. As an example, we give one solitary wave solution of Eq. (20) as follows:

$$\phi_1^I = \phi_{1m}^I \text{sech}^2 \frac{\xi - u_0 \tau}{D}, \quad (23)$$

where $\phi_{1m}^I = \frac{3u_0}{A^-}$, $D = 2\sqrt{\frac{B^-}{u_0}}$, and u_0 is a modulational parameter which can adjust the wave amplitude. In order to compare the solitary wave solution of Eq. (23) with the experimental results, we use the experimental coordinate. By using the Eqs. (14)–(19), we have one incident solitary wave for the particle velocity in the experimental coordinate

$$u^I = u_m^I \text{sech}^2 \frac{x - V^I t + \epsilon P(\eta, \tau)}{D^I}. \quad (24)$$

Similarly, one reflected solitary wave and one transmitted solitary wave for the particle velocity in the experimental coordinate are, respectively, as follows [48,49]:

$$u^R = u_m^R \text{sech}^2 \frac{x - V^R t + \epsilon Q(\xi, \tau)}{D^R}, \quad (25)$$

$$u^T = u_m^T \text{sech}^2 \frac{x - V^T t + \epsilon P(\eta, \tau)}{D^T}, \quad (26)$$

where $u_m^\gamma = u_{m0}^\gamma \exp(-\frac{v_d}{2} t)$, namely $u_m^\gamma = u_{m0}^\gamma \exp(-\frac{v_d}{2C_d} x)$ [48,49], and u_{m0}^γ is the initial wave amplitude. Notice that the amplitude decays exponentially due to the viscosity. However, the amplitude remains a constant if we neglect the viscosity of the dusty plasma, i.e., $v_d = 0$.

There is an arbitrary constant to control the strength of the solitary wave. We can choose this constant as the wave amplitude of u_m^γ . Then both the wave propagation velocity and the wave width depend on the wave amplitude, we have

$$V^\gamma = C_d^\mp + \frac{u_m^\gamma}{2} \quad \text{and} \quad D^\gamma = (1 - \frac{u_m^\gamma}{2C_d^\mp}) \sqrt{\frac{4C_d^\mp}{u_m^\gamma} \lambda_{Dd}^\mp}.$$

For convenience, the standard KdV equation (10) can be translated into general KdV equations (20), (21), and (22) by the transformations of $\phi_1^\gamma = -\frac{6B}{A} \phi$ and $\tau = \frac{1}{B} t$.

III. REFLECTION AND TRANSMISSION AT AN INTERFACE DUE TO INCIDENT WAVE

A. Continuity conditions

Neglecting higher-order quantities, we give the continuity conditions at the interface $x = 0$ for the electric potential, $[\phi^I + \phi^R]_{|x=0} = \phi^T_{|x=0}$, and conservation of the dust fluid momentum $m_d^- n_{d0}^- [u^I + u^R]_{|x=0} = m_d^+ n_{d0}^+ u^T_{|x=0}$ (all physical quantities are in experimental coordinates), we then have

$$\phi^T_{|x=0} = \frac{2}{1 + \chi} \phi^I_{|x=0}, \quad (27)$$

$$\phi^R_{|x=0} = \frac{1 - \chi}{1 + \chi} \phi^I_{|x=0}, \quad (28)$$

where $\chi = \frac{m_d^+ n_{d0}^+ C_d^+ T_{\text{eff}}^-}{m_d^- n_{d0}^- C_d^- T_{\text{eff}}^+}$. Notice from Eq. (27) and Eq. (28) that the “initial conditions” of the transmitted wave and the reflected wave can be given from the incident wave at the interface $x = 0$.

B. Reflection and the transmission due to the incident wave

Suppose that there is an exact incident solitary wave from Eq. (10)

$$\phi^{(I)} = -\frac{2}{D^2} \text{sech}^2 \left(\frac{\xi}{D} - \frac{4\tau}{D^2} \right), \quad (29)$$

it propagates from the region $x < 0$ to the interface at $x = 0$, it will be reflected and transmitted. The equivalent “initial condition” for both the reflected wave and the transmitted waves can be given by the boundary conditions of Eq. (27) and Eq. (28),

$$\phi^{(T)}(t_T, 0) = \frac{A_T}{(L_T)^2} \text{sech}^2 \left(\frac{t_T}{L_T}, 0 \right), \quad (30)$$

$$\phi^{(R)}(t_R, 0) = \frac{A_R}{(L_R)^2} \text{sech}^2 \left(\frac{t_R}{L_R}, 0 \right), \quad (31)$$

where $A_T = 2A_0 \frac{1}{1+\chi} \frac{T_{\text{eff}}^-}{T_{\text{eff}}^+}$, $L_T = L_0$, $A_R = A_0 \frac{1-\chi}{1+\chi}$, and $L_R = L_0$, $A_0 = 2$. As a result, we can obtain the numbers of both the reflected solitary waves and the transmitted solitary waves, as well as the amplitudes of all solitary waves produced by the incident solitary wave.

C. Reflection due to the incident wave

Now we try to know whether there is a reflected solitary wave. The parameter χ can be written in the other form $\chi = \frac{n_{d0}^+}{n_{d0}^-} \sqrt{\frac{\rho^+}{\rho^-}} (\frac{r^+}{r^-})^2$, here we use the results of $m_d^\pm \sim \rho^\pm (r^\pm)^3$ and $Z_d \sim T_{\text{eff}}^\pm r^\pm$ [50,51], where n_{d0}^+ , ρ^+ , and r^+ are the density of the dust particles, density of the dust materials, and the radius of the dust particles in the region $x > 0$, while n_{d0}^- , ρ^- , and r^- are those in the region $x < 0$. The existing condition of the reflected solitary wave is $\chi < 1$, i.e., $(r^-)^2 \sqrt{\rho^-} n_{d0}^- > (r^+)^2 \sqrt{\rho^+} n_{d0}^+$. It seems that whether there is a reflected solitary wave depends on the system parameters such as the dust particle number density, mass of dust particles, and charge of a dust particles in both regions.

D. Transmission due to the incident wave

We now try to know about the transmitted wave due to the incident wave. It is certain that there is at least one transmitted solitary wave. The largest amplitude of the transmitted solitary wave (the first transmitted solitary wave) is $2(\sqrt{A_T + \frac{1}{4}} - \frac{1}{2})L_T^{-2}$. A second transmitted solitary wave may also be produced due to the incident solitary wave. The amplitude of the second transmitted solitary waves is $2(\sqrt{A_T + \frac{1}{4}} - \frac{3}{2})L_T^{-2}$. It seems that no second transmitted solitary wave can be produced when $A_T < 2$. Notice that the numbers of the transmitted solitary waves and their amplitude also depend on the system parameters in both regions.

IV. COMPARISONS WITH THE NUMERICAL AND EXPERIMENTAL RESULTS

The analytical results can be directly compared with the experimental and numerical results. The experiments were performed in the PK-3 Plus laboratory on board the ISS. The detailed description of the set up can be found in Ref. [52]. The argon plasma was produced by a capacitively coupled radio-frequency (rf) discharge at 13.56 MHz. Under microgravity conditions, a binary complex plasma was formed by injecting two types of particles. One of them is melamine formaldehyde particles of a diameter of $2.55 \mu\text{m}$ with a mass $m_b = 1.34 \times 10^{-14}$ kg, while the other is SiO_2 particles of a diameter of $1.55 \mu\text{m}$ with a mass $m_s = 3.6 \times 10^{-15}$ kg. An interface emerged between two different particles as they were phase separated [23]. The motions of individual particles are recorded using video microscopy with a frame rate of 50 frames per second. Here we focus on the part of the cloud above the particle-free central void region. The big particles were confined in the upper part (where we assume that it is in the region $x > 0$), while the small particles were located in the lower part (where we assume that it is in the region $x < 0$). The neutral gas pressure was set as 10 Pa. The solitary

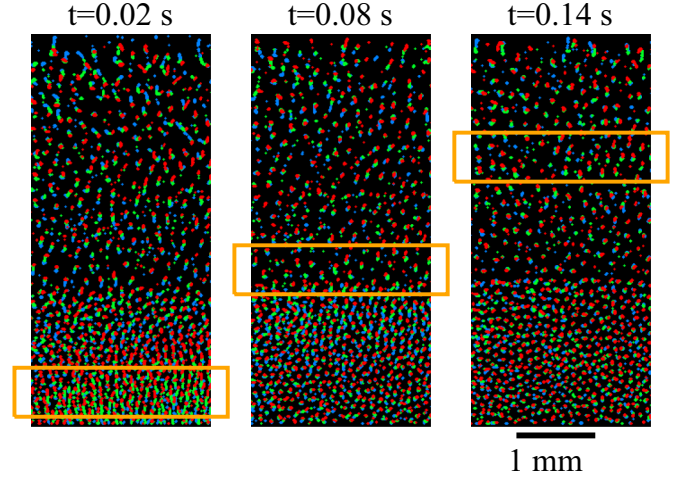


FIG. 1. Propagation of a solitary wave in a phase-separated binary complex plasma in the experiment performed in the PK-3 Plus laboratory on board ISS under microgravity conditions [23]. In each panel, three consecutive recorded images with a interval of 0.02 s are filtered and overlaid and are in blue, green, and red, respectively. The approximate locations of the solitary wave are highlighted by the yellow boxes. Gas pressure is 10 Pa.

wave was excited at the lower boundary using function generator (FG), shown in Fig. 1. In the experiment, the FG was switched off and the particle cloud was pressed downwards. As the cloud hit the edge of the central void, the downwards motion stopped. A quasisolitary wave was instantaneously excited and propagated upwards. The approximate locations of the solitary wave at three time periods (centered at $t = 0.02, 0.08, 0.14$ s) are highlighted by yellow boxes in Fig. 1. The motions of individual small particles close to the lower boundary can be clearly seen as each particle appears as three connecting clusters of pixels in blue, green, and red, representing its trajectory. However, such motions of big particles can be barely visible in the overlaid images after the wave propagates across the interface, accompanied by a dramatic drop of the particle velocity in the wave [53]. Dedicated particle tracking was applied to the experiment analysis in order to obtain the dynamics of individual particles.

The propagation of the solitary wave is revealed in the periodogram in Fig. 3(e) in terms of z velocity v_z . However, this propagation cannot be directly seen via the evolution of the particle number density n in Fig. 3(j), presumably due to the collective motion of the whole particle cloud. The propagation speed was directly estimated as the slope of the trajectory of the solitary wave, highlighted by the dashed lines. As result, the propagation speed in the region composed by small particles was 25 mm/s, while it was 15 mm/s in the region of big particles [23].

Besides the experiments, Langevin dynamics simulations were also performed using LAMMPS [54,55] in microcanonical (NVE) ensemble. The force acting on each particle includes three components. The first component results from the sum of Yukawa interaction with neighboring particles. The second component is the ion drag force directed in the positive z direction. We assumed two constant ion drag forces for small

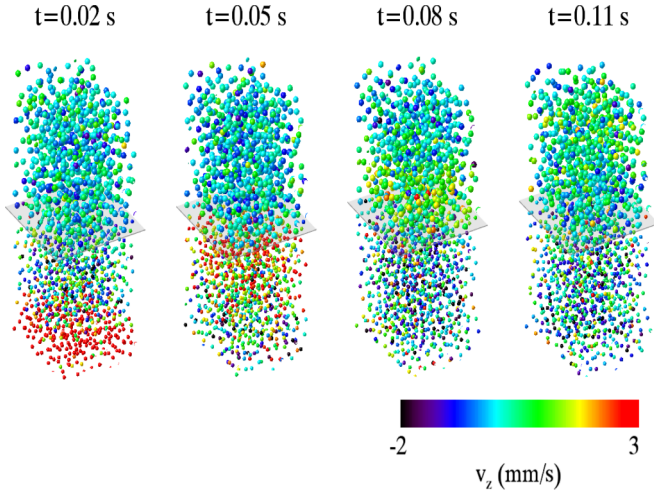


FIG. 2. Propagation of a solitary wave in a phase-separated binary complex plasma in the Langevin dynamics simulation [23]. Gas pressure is 5 Pa. The vertical velocity v_z is exhibited by the color. The interface is marked by a gray square sheet.

and big particles, respectively, leading to a phase-separated binary complex plasma [32]. The third component is associated with the plasma potential, which provides a parabolic confinement. The joint effect of the latter two components confines the particle cloud of two types together and their magnitude determines the gap size at the interface. The heating is implemented via a Langevin heat bath where the temperature is set as $T = 300$ K in the simulation.

The simulations were performed for 4000 small particles and 4000 big particles with periodic boundaries in x and y directions. We chose plasma and particle parameters according to typical parameters in experiments. Two types of particles were selected (the same as in the experiment). The charge for small and big particles are $Q_s = 2700e$ and $Q_b = 4500e$ [23], respectively. In order to study the propagation of solitary wave at low damping regime, we selected another gas pressure of 5 Pa in addition to the pressure achieved in the experiments. The damping rate was calculated based on the Epstein formula for the argon gas [56–58]. They are $\mu_s = 57$ s $^{-1}$ and $\mu_b = 42$ s $^{-1}$ corresponding to a gas pressure 10 Pa [23], while $\mu_s = 28.5$ s $^{-1}$ and $\mu_b = 21$ s $^{-1}$ corresponding to a gas pressure 5 Pa. The Debye lengths in both regions were assumed to be $\lambda_{Dd}^{\pm} = 100$ μm . Note that in reality the discharge conditions change considerably as the gas pressure is lower. The change of the plasma parameters such as the electron temperature and density inevitably leads to the change of the Debye lengths as well as the particle charge [59]. However, to study the impact of damping rate alone and leave out other effects, we simplified the model and assumed that the particle charge and Debye length do not change accordingly.

In the simulation, the particles moved to an equilibrium position from their initial positions, where the small particles were placed close to a piston with big particles above them. The solitary wave was excited by a push of the piston at the lower boundary of the small particles. The form of the piston motion can be described as a sinus function and the push lasted for the first quarter period. The details of the simulation

and the rest of the parameters can be found in Ref. [23]. As result, the propagation of the solitary wave in the simulation is comparable with that in the experiment, see Fig. 2. For a detailed analysis of the propagation characteristics, we divided the particle cloud into cells in z direction and plot the evolution of the averaged v_z over the particles in each cell. The results are shown in Figs. 3(c), 3(d) 3(h), and 3(i). The amplitude of the solitary wave, in terms of the z velocity v_z of individual particles, decreases considerably as it propagates upwards, as also demonstrated in Fig. 2.

If we consider the dissipation effect to all the solitary waves of Eq. (24), Eq. (25), and Eq. (26), then the amplitude of the solitary waves are in the following forms [48,49]:

$$u_m^I = u_{m0}^I \exp\left(-\frac{1}{2}v^-t\right), \quad (32)$$

$$u_m^R = u_{m0}^R \exp\left(-\frac{1}{2}v^-t\right), \quad (33)$$

$$u_m^T = u_{m0}^T \exp\left(-\frac{1}{2}v^+t\right), \quad (34)$$

where u_{m0}^I is the initial wave amplitude at the point $t = 0$ for the incident wave, u_{m0}^R and u_{m0}^T are the “initial wave amplitudes” at the interface for the reflected and the transmitted solitary waves, t is the propagation time, and $v^- = 57$ s $^{-1}$ and $v^+ = 42$ s $^{-1}$ correspond to the case of gas pressure 10 Pa [23] in the region $x < 0$ and $x > 0$, respectively. It seems that the wave amplitude decreases as the wave propagates away.

The maximum dust particle speed (the initial dust particle speed) of the incident wave is $u_{m0}^I \approx 5$ mm/s (see Fig. 3(a) in the Ref. [23]) in the region $x < 0$, then $u_m^I \approx 5 \exp(-28.5t)$ mm/s. We obtain $u_m^I|_{t=t_0} \approx 1.25$ mm/s, the amplitude of the dust particle speed of the incident wave at the interface, where $t_0 = 0.05$ s, which will be the “initial conditions” for both the reflection and the transmission. We then have that $\chi \approx 1.33$ and $A_T \approx 2.1$ by using the above parameter. The reflected wave and the transmitted wave from the incident wave by the interface will be produced. By using the inverse scattering method [43,44], we obtain that there is only one transmitted solitary waves (the amplitude of the second solitary wave is about 0.03, which is so small that it is negligible) with the amplitude $u_m^T|_{t=t_0} = (\sqrt{A_T} + 0.25 - 0.5) \frac{C_D^+ T_{\text{eff}}^+}{C_D^- T_{\text{eff}}^-} u_m^I|_{t=t_0} \approx 0.76 u_m^I|_{t=t_0}$ at the interface ($x = 0, t = t_0$), while there are no reflected solitary wave since $\chi > 1$.

Notice that the continuity condition is not satisfied if we only consider the incident solitary wave and the transmitted solitary wave. Actually reflection exists but results in smaller-amplitude linear waves (radiations or ripples [43,44]). By assuming that $\phi^-|_{x=0} = \phi^I|_{x=0} + \phi^R|_{x=0} + \phi^r|_{x=0}$ in the region $x < 0$ at the interface, and $\phi^+|_{x=0} = \phi^T|_{x=0} + \phi^t|_{x=0}$ in the region $x > 0$, where $\phi^I|_{x=0}$, $\phi^R|_{x=0}$, $\phi^r|_{x=0}$, $\phi^T|_{x=0}$, $\phi^t|_{x=0}$ are the incident solitary wave, the reflected solitary wave, the reflected linear wave, the transmitted solitary wave, and the transmitted linear wave, respectively, we obtain the “initial conditions” of both the reflected linear wave and the transmitted linear wave by using the continuity condition at the interface: $\phi^r|_{x=0} = -\frac{\chi-1}{\chi+1} \phi^I|_{x=0}$, $\phi^t|_{x=0} = 0$, i.e., there are reflected linear waves, but there are no transmitted linear wave. Then we have $u^r|_{x=0} = \frac{1-\chi}{1+\chi} u_m|_{x=0} \text{sech}^2 \frac{V^I(t-t_0)}{D}$.

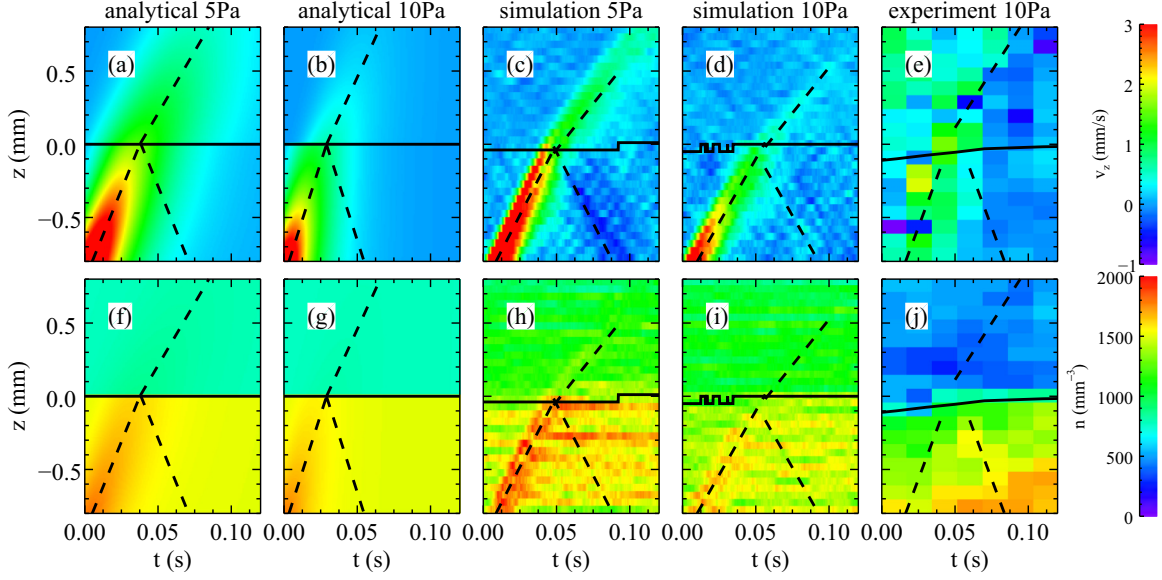


FIG. 3. Propagation characteristics of solitary waves in terms of particle z velocity v_z [(a)–(e)] and number density n [(f)–(j)] in phased-separated binary complex plasmas. The analytical results are shown in columns 1 and 2. The results obtained from Langevin dynamics simulations are shown in columns 3 and 4. The experimental results are shown in column 5.

In order to understand the reflected linear waves, we expand the function of $u^r|_{x=0}$ to cosine series in the region $-\frac{D^l}{V^l} < (t - t_0) < \frac{D^l}{V^l}$ with period of $2\frac{D^l}{V^l}$. We then have

$$u^r|_{x=0} = \frac{1-\chi}{1+\chi} u_m|_{x=0} \left[\frac{a_0}{2} + \sum_{k=1}^{\infty} a_k \cos \frac{k\pi(t-t_0)}{D^l/V^l} \right],$$

where $a_k = \frac{2V^l}{D^l} \int_{t_0}^{t_0 + \frac{D^l}{V^l}} [\text{sech}^2 \frac{V^l(t-t_0)}{D^l}] \cos \frac{k\pi(t-t_0)}{D^l/V^l} dt$, $k = 0, 1, 2, \dots$, from which we obtain $a_0 \approx 0.76$, $a_1 = \int_0^1 \text{sech}^2 y \cos \frac{\pi y}{2} dy \approx 0.5$, $a_2 = \int_0^1 \text{sech}^2 y \cos(\pi y) dy \approx 0.02$. Finally, we have $u^r|_{x=0} = \frac{1-\chi}{1+\chi} u_m|_{x=0} \{0.38 + 0.5 \cos[\omega_0(t - t_0)] + 0.02 \cos[2\omega_0(t - t_0)]\}$ in the region $-\frac{D^l}{V^l} < (t - t_0) < \frac{D^l}{V^l}$, where $\omega_0 = \frac{\pi V^l}{D^l}$.

The reflected radiations can be given approximately as follows: $u^r(x, t) = \frac{1-\chi}{1+\chi} u_m|_{x=0} \{0.38 + 0.5 \cos[k_0 x + \omega_0(t - t_0)] + 0.02 \cos[2k_0 x + 2\omega_0(t - t_0)]\} \exp(-\frac{v_d}{2C_d} |x|)$, where $k_0 = \frac{\omega_0}{C_d}$, $t > t_0$.

The evolutions of incident solitary wave, transmitted solitary wave, and linear reflected wave of our analytical results by particle velocity and the particle number density are shown in Fig. 3. The incident solitary waves by particle velocity is given by Eq. (24) in the region $x < 0$, where $u_{m0}^l = 5$, $v_d = 57 \text{ s}^{-1}$, $V^l = 25 + 2.5 \exp(-28.5t) \text{ mm/s}$, and $D^l = [4.47 - 0.45 \exp(-28.5t)] \exp(14.25t) \lambda_{Dd}^-$. The linear reflected wave by particle velocity is

$$u^r(x, t) = \frac{1-\chi}{1+\chi} u_m|_{x=0} \exp\left(-\frac{v_d}{2C_d} |x|\right) \{0.38 + 0.5 \cos[k_0 x + \omega_0(t - t_0)]\} \text{ (mm/s)} \quad (35)$$

where $t_0 \approx 0.05 \text{ s}$.

In the region $x > 0$, the transmitted solitary wave by particle velocity is given by Eq. (26), where $u_{m0}^T = 0.76$, $v_d = 42 \text{ s}^{-1}$, $V^T = 15 + 0.64 \exp[-21(t - t_0)] \text{ mm/s}$, $D^T = \{6.9 - 0.3 \exp[-21(t - t_0)]\} \exp[10.5(t - t_0)] \lambda_{Dd}^+$, where we have neglected the higher-order term $\epsilon P(\eta, \tau)$ and using the assumption of $\lambda_{Dd}^- = \lambda_{Dd}^+ = 100 \mu\text{m}$.

The evolution of the incident solitary waves by dust particle number density is also shown in Fig. 3, which can be given from Eq. (17) as follows:

$$n^l = 1070 + 214 \exp(-28.5t) \text{sech}^2 \frac{x - V^l t + \epsilon P(\eta, \tau)}{D^l} \text{ (mm}^{-3}\text{)} \quad (36)$$

in the region $x < 0$.

The linear reflected wave by particle number density is given from Eq. (18)

$$n^r(x, t) = \frac{1-\chi}{1+\chi} u_m|_{x=0} \exp\left(-\frac{v_d}{2C_d} |x|\right) \{16.26 + 21.4 \cos[k_0 x + \omega_0(t - t_0)]\} \text{ (mm}^{-3}\text{)} \quad (37)$$

In the region $x > 0$, the transmitted solitary wave by particle number density is from Eq. (19),

$$n^T = 520 + 26.6 u_m^T|_{x=0} \exp[-21(t - t_0)] \text{sech}^2 \frac{x - V^T(t - t_0) + \epsilon P(\eta, \tau)}{D^T} \text{ (mm}^{-3}\text{)}. \quad (38)$$

Using the analytical method, the propagation of the solitary waves is shown in Figs. 3(a), 3(b), 3(f), and 3(g) in terms of z velocity and number density. The results can be directly compared with the numerical simulation and experiments. As we can see in the figure, the solitary waves propagate faster in the small particle region than in the big particle region. The propagation speeds obtained in the theoretical calculations are slighter higher than those in the experiments and numerical simulations. This is resulted possibly from our approximated assumption such as the constant Debye length and the constant dust charge, etc. For $P = 10 \text{ Pa}$ the velocity in z direction decreases rapidly as the solitary wave propagates in the small particle region. The rise of number density in the solitary wave

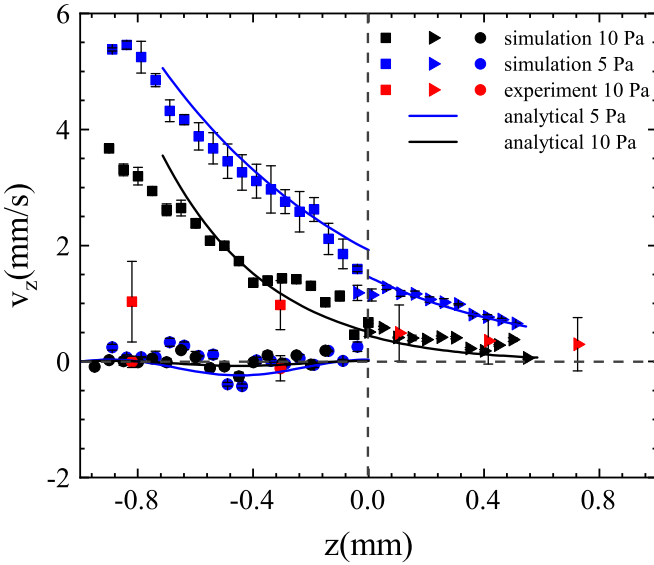


FIG. 4. Particle z velocity v_z in the solitary waves. For the experiments and simulations, v_z in the incident and transmitted waves are shown in square and triangle symbols, respectively, while that in the reflected waves is shown in circle symbols. The analytical results are shown by lines.

is marginal in the small particle region and barely visible in the big particle region. For $P = 5$ Pa the damping rate is much smaller and the z velocity of particles decays in a slower pace. The reflection starts to be visible, particularly in the simulation.

We directly compare the evolution of z velocity of particles in the solitary wave in Fig. 4. To make the five cases directly comparable, we set the propagation time $t = 0$ where the solitary wave front is visible at $z \sim -0.8$ mm in the figure. For both pressures, we see a drop of v_z at the interface as the solitary wave transmits from the small particle region to the big particle region. As to the reflection, the absolute values of v_z are low. The simulation and the analytical results show a reasonable agreement. However, the experimental result shows a clear deviation from the analytical and numerical results, particularly for the incident wave. Nevertheless, as shown in Fig. 1 ($t = 0.02$ s), the z velocity of individual particles at the bottom of the cloud was rather high as the solitary wave was initially excited, exhibited by the elongated trajectory of individual particles. This feature is barely visible in Fig. 1 ($t = 0.14$ s), as the wave reached the big particle cloud. As the mean value and the error bar for the experimental results in Fig. 4 are calculated by the maximal position and the full width at half maximum of the Gaussian fit of the particle velocity in the selected cell, they may be underestimated to some extent. This presumably was caused by the limited temporal and spatial resolution of the cameras equipped in the PK-3 Plus laboratory and unfortunately can not be further improved. Further careful experimental investigations with higher temporal resolution are required to obtain a more precise results.

The total energy of a solitary wave in a dusty plasma includes both the kinetic energy and the potential energy, which

depend on the solitary wave amplitude. It is found that the solitary wave amplitude decays exponentially with time in the presence of collision and, therefore, it seems that the energy of a solitary wave decreases with time in the presence of collision. However, the total energy of the system includes not only the kinetic energy, the potential energy of all solitary waves but also the linear radiation energy and the thermal energy of the system. The sum of all the solitary wave energies, the thermal energy, and the linear radiation energy of the system is conserved.

V. CONCLUSION

Inspired by the experimental observations in the PK-3 Plus Laboratory on board the ISS, we have theoretically investigated the propagation of a solitary wave across an interface in a binary complex plasma. By using the traditional reductive perturbation method, we obtain three KdV equations to represent the incident solitary wave, the transmitted solitary wave and the reflected solitary wave. Based on the continuity conditions at the interface, we obtain the equivalent “initial conditions” for both the transmitted nonlinear wave and the reflected waves from the incident wave. We further obtain the numbers of the reflected and the transmitted solitary waves as well as all the wave amplitudes by using the inverse scattering method. The ripples of both reflection and transmission have also been given by using the Fourier series. It is found that the number of the reflected and the transmitted solitary waves, all the wave amplitudes and the ripples of both reflection and transmission depend on the system parameters such as the number density, electric charge, mass of the dust particles as well as the effective temperature in both regions. The analytical results can explain the experimental and numerical results, though there are differences between the analytical results and the experimental ones which is possibly due to the approximated assumption of several constant parameters such as the Debye length, dust charge, as well as the approximation of the equation of state.

The method and the results of the present paper can also be applied to the other Yukawa system, such as liquid metals, liquid metallic hydrogen, helium, screening of thermonuclear reaction rates in astrophysical settings, and colloidal suspensions. For the nonuniform Yukawa system, by measuring the information of the reflected wave and the transmitted wave by an incident pulse, we can determine the information of the discontinuous regions and the system parameters, such as the plasma number density, dust size, and dust charge, for a dusty plasma.

ACKNOWLEDGMENTS

This work was supported by the National Natural Science Foundation of China (NSFC) under Grants No. 11965019, No. 11847142, No. 11975073, No. 12035003, No. 12165018, No. 11765017, and No. 12047574. We thank H. M. Thomas for the helpful comments.

- [1] M. Horányi, *Annu. Rev. Astron. Astrophys.* **34**, 383 (1996).
- [2] D. A. Mendis and M. Rosenberg, *Annu. Rev. Astron. Astrophys.* **32**, 419 (1994).
- [3] N. N. Rao, P. K. Shukla, and M. Y. Yu, *Planet. Space Sci.* **38**, 543 (1990).
- [4] A. Barkan, R. L. Merlino, and N. D'Angelo, *Phys. Plasmas* **2**, 3563 (1995).
- [5] W. S. Duan, G. X. Wan, X. Y. Wang, and M. M. Lin, *Phys. Plasmas* **11**, 4408 (2004).
- [6] P. K. Shukla and B. Eliasson, *Phys. Rev. E* **86**, 046402 (2012).
- [7] S. Ghosh, M. R. Gupta, N. Chakrabarti, and M. Chaudhuri, *Phys. Rev. E* **83**, 066406 (2011).
- [8] Y. Choi, G. Dharuman, and M. S. Murillo, *Phys. Rev. E* **100**, 013206 (2019).
- [9] P. K. Shukla and V. P. Silin, *Phys. Scr.* **45**, 508 (1992).
- [10] U. de Angelis, V. Formisano, and M. Giordano, *J. Plasma Phys.* **40**, 399 (1988).
- [11] G. E. Morfill and H. Thomas, *J. Vac. Sci. Technol. A* **14**, 490 (1996).
- [12] A. Barkan, N. D'Angelo, and R. L. Merlino, *Planet. Space Sci.* **44**, 239 (1996).
- [13] N. D'Angelo and B. Song, *Planet. Space Sci.* **38**, 1577 (1990).
- [14] A. Melzer, S. Nunomura, D. Samsonov, Z. W. Ma, and J. Goree, *Phys. Rev. E* **62**, 4162 (2000).
- [15] S. Nunomura, J. Goree, S. Hu, X. Wang, and A. Bhattacharjee, *Phys. Rev. E* **65**, 066402 (2002).
- [16] K. Avinash, P. Zhu, V. Nosenko, and J. Goree, *Phys. Rev. E* **68**, 046402 (2003).
- [17] X. Wang, A. Bhattacharjee, and S. Hu, *Phys. Rev. Lett.* **86**, 2569 (2001).
- [18] H. Zhang, Y. Yang, X. R. Hong, X. Qi, W. S. Duan, and L. Yang, *Phys. Rev. E* **95**, 053207 (2017).
- [19] Y. Y. Tsai, J. Y. Tsai, and L. I, *Nat. Phys.* **12**, 573 (2016).
- [20] S. Hussain and H. Hasnain, *Phys. Plasmas* **24**, 032106 (2017).
- [21] W. Lin, M. S. Murillo, and Y. Feng, *Phys. Rev. E* **100**, 043203 (2019).
- [22] M. Marciante and M. S. Murillo, *Phys. Rev. Lett.* **118**, 025001 (2017).
- [23] W. Sun, M. Schwabe, H. M. Thomas, A. M. Lipaev, V. I. Molotkov, V. E. Fortov, Y. Feng, Y. F. Lin, J. Zhang, Y. Guo, and C. R. Du, *Europhys. Lett.* **122**, 55001 (2018).
- [24] C. R. Du, V. Nosenko, H. M. Thomas, Y. F. Lin, G. E. Morfill, and A. V. Ivlev, *Phys. Rev. Lett.* **123**, 185002 (2019).
- [25] F. Wieben, J. Schablinski, and D. Block, *Phys. Plasmas* **24**, 033707 (2017).
- [26] P. Hartmann, Z. Donkó, G. J. Kalman, S. Kyrkos, K. I. Golden, and M. Rosenberg, *Phys. Rev. Lett.* **103**, 245002 (2009).
- [27] B. Smith, T. Hyde, L. Matthews, J. Reay, M. Cook, and J. Schmoke, *Adv. Space Res.* **41**, 1510 (2008).
- [28] A. Wysocki, C. R. R. Räth, A. V. Ivlev, K. R. Sütterlin, H. M. Thomas, S. Khrapak, S. Zhdanov, V. E. Fortov, A. M. Lipaev, V. I. Molotkov, O. F. Petrov, H. Löwen, and G. E. Morfill, *Phys. Rev. Lett.* **105**, 045001 (2010).
- [29] K. Jiang, L. J. Hou, A. V. Ivlev, Y. F. Li, C. R. Du, H. M. Thomas, G. E. Morfill, and K. R. Sütterlin, *Europhys. Lett.* **93**, 55001 (2011).
- [30] C. R. Du, K. R. Sütterlin, K. Jiang, C. R. Räth, A. V. Ivlev, S. Khrapak, M. Schwabe, H. M. Thomas, V. E. Fortov, A. M. Lipaev, V. I. Molotkov, O. F. Petrov, Y. Malentschenko, F. Yurtschichin, Y. Lonchakov, and G. E. Morfill, *New J. Phys.* **14**, 073058 (2012).
- [31] A. V. Ivlev, S. K. Zhdanov, H. M. Thomas, and G. E. Morfill, *Europhys. Lett.* **85**, 45001 (2009).
- [32] C. Killer, T. Bockwoldt, S. Schütt, M. Himpel, A. Melzer, and A. Piel, *Phys. Rev. Lett.* **116**, 115002 (2016).
- [33] L. Yang, M. Schwabe, S. Zhdanov, H. M. Thomas, A. M. Lipaev, V. I. Molotkov, V. E. Fortov, J. Zhang, and C. R. Du, *Europhys. Lett.* **117**, 25001 (2017).
- [34] D. J. Korteweg and G. de Vries, *Phil. Mag.* **39**, 422 (1895).
- [35] M. Schwabe, S. K. Zhdanov, H. M. Thomas, A. V. Ivlev, M. Rubin-Zuzic, G. E. Morfill, V. I. Molotkov, A. M. Lipaev, V. E. Fortov, and T. Reiter, *New J. Phys.* **10**, 033037 (2008).
- [36] M. Schwabe, S. A. Khrapak, S. K. Zhdanov, M. Y. Pustynnik, C. R. R. Räth, M. Fink, M. Kretschmer, A. M. Lipaev, V. I. Molotkov, A. S. Schmitz, M. H. Thoma, A. D. Usachev, A. V. Zobnin, G. I. Padalka, V. E. Fortov, O. F. Petrov, and H. M. Thomas, *New J. Phys.* **22**, 083079 (2020).
- [37] S. Jaiswal, M. Y. Pustynnik, S. Zhdanov, H. M. Thomas, A. M. Lipaev, A. D. Usachev, V. I. Molotkov, V. E. Fortov, M. H. Thoma, and O. V. Novitskii, *Phys. Plasmas* **25**, 083705 (2018).
- [38] K. O. Menzel, O. Arp, and A. Piel, *Phys. Rev. Lett.* **104**, 235002 (2010).
- [39] Y. Feng, W. Lin, W. Li, and Q. L. Wang, *Phys. Plasmas* **23**, 093705 (2016).
- [40] W. Li, W. Lin, and Y. Feng, *Phys. Plasmas* **24**, 043702 (2017).
- [41] D. Huang, W. Li, W. Lin, and Y. Feng, *Phys. Plasmas* **24**, 093707 (2017).
- [42] Y. Feng, J. Goree, and B. Liu, *Phys. Rev. Lett.* **109**, 185002 (2012).
- [43] T. Kawahara, *J. Phys. Soc. Jpn.* **41**, 1402 (1976).
- [44] W. S. Duan, B. R. Wang, and R. J. Wei, *Phys. Rev. E* **55**, 1773 (1997).
- [45] C. H. Su and R. M. Mirie, *J. Fluid Mech.* **98**, 509 (1980).
- [46] A. Jeery and T. Kawahara, *Asymptotic Methods in Nonlinear Wave Theory* (Pitman Books Ltd, London, UK, 1982).
- [47] J. Zhang, Y. Yang, Y. X. Xu, L. Yang, X. Qi, and W. S. Duan, *Phys. Plasmas* **21**, 103706 (2014).
- [48] D. N. Gao, H. Zhang, J. Zhang, Z. Z. Li, and W. S. Duan, *Phys. Plasmas* **24**, 043703 (2017).
- [49] S. Ghosh, T. K. Chaudhuri, S. Sarkar, M. Khan, and M. R. Gupta, *Phys. Rev. E* **65**, 037401 (2002).
- [50] B. S. Xie, K. F. He, and Z. Q. Huang, *Phys. Lett. A* **247**, 403 (1998).
- [51] A. Barkan, N. D'Angelo, and R. L. Merlino, *Phys. Rev. Lett.* **73**, 3093 (1994).
- [52] H. M. Thomas, G. E. Morfill, V. E. Fortov, A. V. Ivlev, V. I. Molotkov, A. M. Lipaev, T. Hagl, H. Rothermel, S. A. Khrapak, R. K. Suetterlin, M. Rubin-Zuzic, O. F. Petrov, V. I. Tokarev, and S. K. Krikalev, *New J. Phys.* **10**, 033036 (2008).
- [53] As the big particles above the interface move rather slowly, the clusters of pixels in red (representing the particle in the last frame) cover those in blue and green in the overlaid image of a time span of 0.06 s. The full trajectory of the quasistationary particles cannot be resolved in the processed images and therefore one sees mainly red particles in the figure.
- [54] S. Plimpton, *J. Comput. Phys.* **117**, 1 (1995).
- [55] LAMMPS, <https://lammps.sandia.gov>.

- [56] P. S. Epstein, [Phys. Rev.](#) **23**, 710 (1924).
- [57] U. Konopka, Wechselwirkungen geladener Staubteilchen in Hochfrequenzplasmen, Ruhr-Universität-Bochum, Ph.D. thesis, 2000.
- [58] B. Liu, J. Goree, V. Nosenko, and L. Boufendi, [Phys. Plasmas](#) **10**, 9 (2003).
- [59] K. Takahashi, Y. Hayashi, and S. Adachi, [J. Appl. Phys.](#) **110**, 013307 (2011).